Minimum-Energy Hypersonic Nose and Leading-Edge Shapes

ROGER J. FUREY*
Naval Ship Research and Development Center, Carderock, Md.

Through the gradient method, the Pontryagin maximum principle, is applied to a system of first-order differential equations governing the heat transfer (convection and shock layer radiation) and pressure drag of an axisymmetric or two-dimensional body in hypersonic flow. Numerically determined optimum shapes with given ratios of fineness or thickness are found for minimum drag, minimum heat transfer (convection), minimum heat transfer (radiation), and minimum energy. Minimum energy shapes are found which minimize the sum of convection plus drag work, convection plus radiation plus drag work, and convection plus radiation. The axisymmetric cases produced a near $\frac{3}{4}$ power-law profile for the minimum drag shape and a flat-faced nose for the minimum heat transfer considering convection alone. The optimum-nose shape for a minimum of radiation heating was found to be conical with a cusped tip. The minimum energy shapes were found to result in various combinations of these forms. The over-all results clearly illustrate the geometric means of alleviating the various energy forms. Drag reduction is produced by a slight degree of blunting near the tip. The effect of radiation is concentrated near the tip where the tendency is toward a cone, and minimum convection tends toward the blunted face.

Nomenclature

C_p = specific heat at constant pressure (Btu/lb °R) also pressure coefficient
C_v = specific heat at constant volume (Btu/lb °R)
D = pressure drag, lb; also base diameter, ft
H = Hamiltonian function
h = enthalpy (Btu/lb), also coordinate parameter
L = characteristic length
M_∞ = Mach number
N_α = convection parameter
N_Γ = radiation parameter
Pr = Prandtl number
p = pressure
$\mathbf{R}$ = radius of curvature
R = gas constant (Btu/lb °R)
$\bar{r}, r$ = body coordinate and $\bar{r}/\bar{r}_b$, respectively
$\bar{r}_b$ = base radius
S = entropy (Btu/°R)
$\bar{s}, s$ = body coordinate and $\bar{s}/\bar{r}_b$, respectively
T = temperature, degree absolute (R)
U_∞ = freestream velocity
u, v = local velocities parallel and normal to body surface, fps
w = $\mu/\mathbf{RT}$
$\bar{x}, x$ = axial-body coordinate, ft, and $\bar{x}/\bar{r}_b$, respectively
$\bar{y}, y$ = normal coordinate and $\bar{y}/\bar{r}_b$, respectively
Z = control variable
α = state variable representing convective heating
α_p = Planck absorption coefficient
$\bar{\alpha}$ = absorption coefficient in empirical representation of Planck coefficient (ft²/lb °R⁵)
β = state variable representing pressure drag
Γ = state variable representing radiation heating
γ = specific heat ratio
δ = shock-layer thickness
η = state variable related to convection
θ = angle between shock slope and axis
μ = viscosity coefficient (lb sec/ft²)
ρ = density
σ = Stefan-Boltzmann constant (Btu/hr ft² °R⁴)
ψ = stream function and coordinate
$(\cdot)$ = d/ds

Subscripts

b, e = body surface and boundary-layer edge
o, r = stagnation point and reference conditions
s = conditions just inside shock
t = total conditions
1, 2 = upstream and downstream of normal shock
∞ = freestream conditions

Superscripts

f = end conditions in maximum principle formulation
0 = initial conditions in maximum principle formulation

Presented as Paper 70–825 at the AIAA 5th Thermophysics Conference, Los Angeles, Calif. June 29–July 1, 1970; submitted August 28, 1970; revision received August 30, 1971.

* Assistant Division Head, Aerodynamics Div., Aviation and Surface Effects Department. Member AIAA.

Introduction

SINCE hypersonic vehicles will be required to sustain large heat loads for most of their flight time, both drag and heat transfer should be accounted for in determining their optimum shapes. Previous investigations[1–6] have shown that the geometric shape leading to minimum drag at hypersonic speeds is a slender near conical shape while the flat-faced profile results in minimum heat rate. The compromise required between these opposing geometric shapes leads to the concept of a minimum energy shape. Numerical optimization methods are well suited to this type of problem and have been applied, by the author, in a previous study to determine the minimum energy shape for a hypersonic body with a given base diameter and meridian-arc length.

In the present study, the author attempts to determine the minimum energy nose and leading-edge shapes for the more practical geometric restrictions of given fineness and thickness ratios. Radiation heating was included in the analysis because of its possible contribution to a less blunt minimum energy shape and resulting improvement in performance. Although radiation heating is a small part of the over-all heating in a cruise vehicle (maximum Mach number on the order of 20–25), it could be comparable to convective heating and would eventually exceed it at the velocities required for superorbital vehicles. A compromise would then be required between the blunt shape for convection and the slender shape for radiation.

The problem is approached by setting up a system of first-order ordinary differential equations governing the variables of interest in the form of a Mayer problem in the calculus of variations. A numerical application of the Pontryagin maximum principle is employed and the optimum shapes determined. A geometrical restriction of a given fineness ratio is imposed on the nose and leading-edge shapes. The optimum shapes include minimum drag (pressure drag), minimum heat transfer (convection), minimum heat transfer (radiation), minimum energy (convection + drag), minimum energy (convection + radiation + drag), and minimum energy (convection + radiation).

The flowfield analysis is made under the assumptions of an optically thin gas and a physically thin shock layer. The modified Newtonian theory provides surface-pressure distribution, and centrifugal effects account for pressure variation through the shock layer. A first approximation of the flowfield is obtained on the basis of an isoenergetic condition in the shock layer. The effect of radiation cooling on the temperature distribution is calculated and radiative heating to the body determined. Convective heating is obtained with the condition that the wall temperature is much less than that at the edge of the boundary layer, thus allowing a similarity solution to the boundary-layer equations. The low-wall temperature is consistent with a black-body assumption concerning the radiative heating.

Formulation of Problem

The model used employs the assumption of an inviscid shock layer. The basic hypersonic condition $M_\infty \gg 1$ is employed to justify the assumption that the shock layer is physically thin with the shock wave closely conforming to the body contour. The system of first-order differential equations governing the variables of interest is obtained as follows.

Aerodynamic Heating

The coordinate system is shown in Fig. 1 with s, the distance measured along the body surface from the stagnation point, as the independent variable. The local laminar convective heat-transfer rate is given[7] by

$$q_c = 0.5(Pr)^{-2/3}[(\rho_e\mu_e)_0]^{1/2}U_\infty{}^{1/2}h_t\bar{r}_b{}^{-1/2}F(s)$$

where

$$F(s) = \left(\frac{1}{2}\right)^{1/2}\left(\frac{p}{p_0}\right)\left(\frac{u}{U_\infty}\right)\left(\frac{w_e}{w_{e0}}\right)r^j \Big/ \left[\int_0^s \left(\frac{p}{p_0}\right)\left(\frac{u}{U_\infty}\right)\left(\frac{w_e}{w_{e0}}\right)r^{2j}ds\right]^{1/2} \tag{1}$$

The coordinates are considered as dimensionless through division by the base radius, and $j = 1, 0$ refers to the axisymmetric or two-dimensional case, respectively.

The total heat transferred to a given body per unit time is determined by

$$Q_c = (2\pi)^j\bar{r}_b\bar{r}_b{}^j\int_0^s r^j q_c ds$$

Assuming $w_e \simeq w_{e0}$, we then have

$$\dot{\alpha} \equiv d/ds[Q_c/Pr^{-2/3}(2)^{1/2}(2\pi)^j(\rho_e\mu_e)_0{}^{1/2}U_\infty{}^{1/2}h_t\bar{r}_b{}^{j+1/2}] = (p/p_0)(u/U_\infty)r^{2j}/\eta^{1/2} \tag{2}$$

where

$$\eta = \int_0^s (p/p_0)(u/U_\infty)r^{2j}ds \tag{3}$$

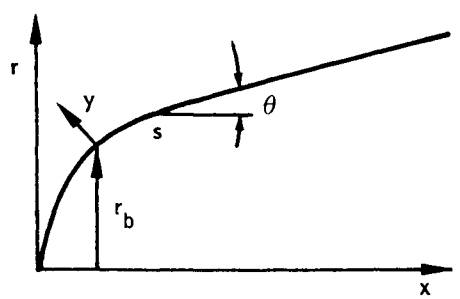

Fig. 1 Body-oriented coordinate system.

The body-surface pressure will be determined through the modified Newtonian relation: $C_p = C_{p0}\sin^2\theta$, for $M_\infty \gg 1$, $p_\infty/p_0 \ll p/p_0$. Then $(p/p_0) \simeq Z^2$ where $Z \equiv dr/ds = \sin\theta$.

Equations (2) and (3) can then be expressed as

$$\dot{\alpha} = (u/U_\infty)Z^2 r^{2j}/\eta^{1/2} \text{ and } \dot{\eta} = (u/U_\infty)Z^2 r^{2j} \tag{4}$$

It remains to determine the local-velocity ratio in a convenient form. This will be delayed until consideration of the shock-layer radiation terms.

Aerodynamic Drag

In the body-oriented coordinate system of Fig. 1, the pressure drag of an arbitrary body can be expressed as

$$\beta \equiv \left[\frac{D}{(2\pi)^j\bar{r}_b\bar{r}_b{}^j p_0}\right] = \int_0^s \left(\frac{p}{p_0} - \frac{p_\infty}{p_0}\right)r^j Z ds \tag{5}$$

On the assumption that $p_\infty/p_0 \ll p/p_0$ in the nose region, the drag relation becomes:

$$\dot{\beta} = Z^3 r^j \tag{6}$$

Shock Layer

The radiation term in the energy equation for an optically thin gas[8] is

$$\nabla \cdot q_r = 4\alpha_p\sigma T^4 \tag{7}$$

Unlike the equations related to convective heating [Eq. (4) and pressure drag Eq. (6)] wherein the history of the variables is needed on the body surface only, the temperature distribution of Eq. (7) is needed throughout the shock layer. The numerical-optimization procedure to be used necessitates recalculating the shock-layer properties (in those problems where radiation is being considered) after each iteration, with each resultant new shape closer to the optimum. Since there are many intermediate shapes between the initial assumed optimum and the final optimum shape, a direct and rapid calculation of the shock-layer properties is a must in order to keep machine time within reason. The shock-layer model to be used will be similar to that of Freeman[9] but modified to avoid the possibility of a free layer (negative pressure on the body surface) inherent in his treatment on some types of bodies.

The treatment of the radiation terms is based on the following assumptions: 1) gas in local thermodynamic equilibrium, 2) optically thin gas, 3) transparent shock and black wall, and 4) perfect gas.

The conservation equations in boundary-layer type coordinates consistent with Fig. 1 are[10]

$$\text{mass} \quad \partial/\partial s\,(r^j\rho u) + \partial/\partial y\,(hr^j\rho v) = 0 \tag{8}$$

$$s\text{-momentum} \quad (u/h)\,\partial u/\partial s + v\,\partial u/\partial y + uv\kappa = -(1/h\rho)\,\partial p/\partial s \tag{9}$$

$$y\text{-momentum} \quad (u/h)\,\partial v/\partial s + v\,\partial v/\partial y - u^2\kappa = -(1/\rho)\,\partial p/\partial y \tag{10}$$

$$\text{energy} \quad \rho T[(u/h)\,\partial S/\partial s + v\,\partial S/\partial y] = -\nabla\cdot q_r \tag{11}$$

Through the introduction of a stream-function ψ, the continuity equation is satisfied directly.

$$\partial\Psi/\partial s = -hr^j\rho v,\ \partial\Psi/\partial y = r^j\rho u \tag{12}$$

Transforming to a Von Mises coordinate system, i.e., $(s,y)\rightarrow(s,\Psi)$, (Fig. 2) and applying the assumptions of the thin shock-layer approximation, i.e., $v \ll u$.

Eqs. (9–11) reduce to

$$u\partial u/\partial s = -1/\rho\partial p/\partial s \tag{13}$$

$$r^j\partial p/\partial\Psi = u\kappa \tag{14}$$

$$\rho T(u/h)\partial S/\partial s = \nabla\cdot q_r \tag{15}$$

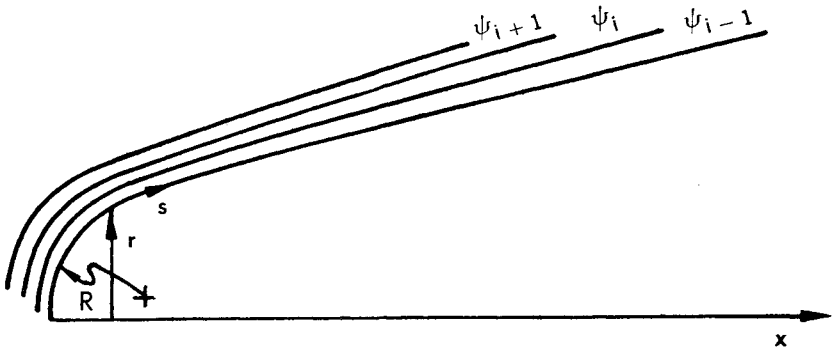

Fig. 2 Von Mises coordinate system.

where, from Eq. (7), Eq. (15) becomes

$$(1/h)\partial S/\partial s = -4\alpha_p \sigma T^4/\rho u T \tag{16}$$

By definition, the optical thickness is $\tau \equiv \int \alpha_p d\ell \simeq \bar{\alpha}_p L$. Near the stagnation point where radiation will be greatest, the shock relations provide $\rho_1 U_1 = \rho_2 U_2$. And as $M_\infty \to \infty$, $\gamma \to 1 \Rightarrow C_p \sim C_v$; also $h = 1 + y/R \simeq 1$.

Substituting into Eq. (16), we obtain

$$\partial/\partial s\,(S/C_v) \approx 4(\tau/L)(\sigma T_2{}^4/\rho_\infty U_\infty C_p T_2) \tag{17}$$

The first expression in parentheses on the right-hand side of Eq. (17) is referred to as the optical depth and the second is the inverse of the Boltzmann number. For optically thin gases and moderate hypersonic Mach numbers, these parameters are quite small implying

$$\partial/\partial s\,(S/C_v) \cong 0 \tag{18}$$

or the entropy is constant along streamlines. The implication here is that the shock-layer properties can be determined through the momentum [Eqs. (13) and (14)] and the equation of state, and, having the temperature distribution, the radiation heating can be determined without ever considering radiation in the conservation equations. The effect here would be to overestimate the radiative contribution (however slightly) by neglecting the radiative cooling within the shock layer and the resultant-temperature decrease. A more reasonable approach would involve first determining the pressure and velocity distributions and then using these values to determine temperature distributions while including radiation. The validity of such an approach is borne out by the results of Ref. 11; Wang applied the thin shock-layer series approximation of Freeman and showed that, to a first approximation, the velocity and pressure distribution within the shock layer are not affected by radiation. This approach is further justified on the basis of other results that concerned considerably higher-radiation levels than in the present problem. It has been observed[12] that the radiation serves to lower the local temperature while increasing the density but that it has little effect on the velocity and pressure distribution.

The approach used here, then, is to deal with Eqs. (13) and (14) on the basis of the isoenergetic implications of Eq. (18). Once the necessary distribution of shock-layer variables is determined, Eq. (16) is solved to obtain the desired temperature distribution while including the effects of radiative cooling.

Proceeding on this basis, Eq. (13) can be expressed as:

$$(p_2/p_2{}^\gamma)^{1/\gamma} \int_{p_2}^{p} p^{1/\gamma}\, \partial p/\partial s\, ds = -\int_{\beta_2 s}^{u} u\, \partial u/\partial s\, ds \tag{19}$$

where the reference pressure and density are those values existing in the stagnation region. The integration here then is dealing with the body-wetting streamline. The lower limit of integration for the velocity term $\beta_2 s$ is based on the fact that in the stagnation region, the velocity varies linearly with distance. The value of β_2, i.e., $\beta_2/U_\infty = 1.268\ (\rho_1/\rho_2)^{1/2}/D$ (Ref. 10) is found to hold for a variety of shapes from spherical to flat faced—both axisymmetric and two-dimensional. Since the pressure p_2 is pretty much constant in the stagnation region, the corresponding lower limits are not inconsistent.

Consider now the momentum relation across a normal shock at the stagnation point. The dynamic pressure on the upstream side and the static pressure on the downstream side can be said to be dominant at extreme Mach numbers. Two conclusions can be drawn from this condition, i.e.,

$$p_{t_2} \simeq p_2 \text{ and } p_2/\rho_2 U_\infty{}^2 \approx \rho_1/\rho_2 \tag{20}$$

where $\rho_1/\rho_2 \approx (\gamma - 1)/(\gamma + 1)$ for $M_\infty \gg 1$.

Utilizing these conditions Eq. (19) can be integrated and reduced to

$$u/U_\infty = \{(\beta_2 s/U_\infty)^2 + 2\gamma/(\gamma + 1)[1 - Z^{\,2(\gamma-1)/\gamma}]\}^{1/2} \tag{21}$$

Equation (21) provides the velocity variation along the body-wetting streamline and, together with Eq. (4), provides the necessary forms for dealing with the convective heating in the Mayer problem formulation. (The independent variable s in this equation is not varied throughout its range but only for the duration of the initial curvature existing at the stagnation point.) It remains to determine the flow properties through the shock layer so as to deal with the radiative heating.

Maslen[13] used Eq. (14) to determine the shock-layer properties by treating the problem through the inverse method. On assuming a shock shape, he used the shock relations to provide the variables just inside the shock wave. The pressure gradient through the shock layer (as provided by Eq. (14) using values from the shock relations) is assumed constant. Integration proceeds from the shock to the body, with $\Psi = 0$ determining the body shape for the assumed shock. A similar procedure will be used in the present application except that the integration will proceed from body to shock. The Newtonian relation and Eq. (21) provide the values of the necessary variables and boundary conditions at the body surface. As with the Maslen method, the pressure gradient will be considered constant across the shock layer.

Eq. (14)

$$\int_{p_b}^{p} dp = \int_{\Psi_0}^{\Psi} (u/r^j R)\, d\Psi = (\rho_\infty U_\infty/R) u \int_0^s Z\, ds \tag{22}$$

where the thin shock-layer conditions have been used to change the integration variable. Utilizing Eq. (21) in the form $(u/U_\infty) = f(s, Z)$, Eq. (22) can be integrated to provide

$$p(s, s_s)/\rho_\infty U_\infty{}^2 = Z^2 + f(s, Z)/R \int_0^s Z ds \tag{23}$$

where the modified Newtonian relation has been used to provide the pressure on the body surface. The Ψ dependence of the pressure is accounted for by the subscripted s_s which refers to the entry point of a particular streamline into the shock layer. The entropy level for a particular streamline can

be determined from the shock relations.[14] Then $\rho = f(\Psi)p^{1/\gamma}$ which, together with Eq. (23), will provide the density distribution through the shock layer.

The velocity at the shock wave is provided by the constancy of the tangential-velocity component across the shock, i.e., $u_s/U_\infty = \cos\theta \simeq (1 - Z^2)^{1/2}$. From Eq. (12) or, what amounts to the same thing, a mass balance at each station s

$$\Psi = (1/1 + j)\rho_\infty U_\infty r^{1+j} = \int_0^\delta r^j \rho u dy \tag{24}$$

In difference form

$$\nabla\Psi_i = (1/1 + j)\rho_\infty U_\infty (r_{b_i}{}^{1+j} - r_{b_{i-1}}{}^{1+j}) = r^j \rho u \Delta y \tag{25}$$

where $u = u_b + (\sum\Delta\Psi_i/\Psi_s)(u_s - u_b)$ at $s =$ constant will provide the corresponding variation of y and the shock-layer thickness. The effects of radiation cooling on the shock-layer temperature distribution can now be determined through the energy equation including the radiation term. The entropy variation can be expressed as

$$p/\rho^\gamma = (p_r/\rho_r{}^\gamma)\exp(S - S_r/C_v) \text{ for } \gamma \to 1 \Rightarrow T \simeq T_r \exp(S - S_r/C_v) \tag{26}$$

Therefore $\partial/\partial s(S/C_v) = (1/T\ \partial T/\partial s)$ and Eq. (16) becomes

$$\partial T/\partial s = -4\alpha_p \sigma T^4/\rho u C_v \tag{27}$$

The absorption coefficient can be expressed as $\alpha_p = \bar{\alpha}_p\ \rho^a T^b$ where a and b are determined from opacity data ($a = 1$, $b = 5$, accurate for $T \leq 15{,}000°\text{K}$; Ref. 11). The energy equation then becomes $\partial T/\partial s = -4\bar{\alpha}_p \sigma T^{4+b}/uC_v$.

Separating the variables and integrating results in

$$T(s, s_s)/T(s_s) = [1 + 4(3 + b)\bar{\alpha}_p \sigma/C_v[T(s_s)]^{3+b}\int_{s_s}^{s} ds/u]^{-\frac{1}{3+b}} \tag{28}$$

where the subscripted variable s_s again refers to the entry point of a particular streamline into the shock layer.

Radiative Heating

With the temperature distribution throughout the shock layer available, it is now possible to determine the radiation-heating level to the body. From $\partial q_r/\partial y = 2\alpha_p \sigma T^4$, applying Von Mises transformation and integrating

$$q_r = \int_0^\Psi 2\alpha_p \sigma T^4/r^j \rho u\, d\Psi$$

utilizing $\alpha_p = \bar{\alpha}_p \rho^a T^b$, $d\Psi = \rho_\infty U_\infty r_b{}^j Z ds$ and arranging so as to determine the total radiative heating to the body per unit time, we obtain

$$\dot{\Gamma} \equiv d/ds[Q_r/2(2\pi)^j \bar{\alpha}_p \sigma \rho_\infty \bar{r}_b{}^{2+j} T_t{}^{4+b}] = r^j \lambda \tag{29}$$

where

$$\dot{\lambda} = Z\bar{T}^{4+b}/\bar{u} \tag{30}$$

and we have introduced

$$\bar{T} = 1/\delta \int_0^\delta (T/T_t)dy \text{ and } \bar{u} = 1/\delta \int_0^\delta (u/U_\infty)dy$$

Treating the radiation terms in this manner, that is, taking mean values of temperature and velocity at a given station, amounts to treating the radiation as a distribution of sources along the shock layer.

The introduction of the total temperature T_t into Eq. (29), together with the previously mentioned dimensionless coordinates, produces a dimensionless energy term just as in Eqs. (2) and (5). Equation (5) is seen to be in terms of energy by multiplying the numerator and denominator of the left-hand side by the freestream velocity U_∞. It remains to relate the various energy terms through a common denominator.

Parameters Relating Energy Forms

The energy levels of convective heating, radiative heating, and the work done by pressure drag will, of course, vary with Mach number and altitude. This will be accounted for by introducing the parameters

$$N_\alpha = \frac{[(\rho_e \mu_e)_0]^{1/2} U_\infty{}^{5/2}}{\bar{r}_b{}^{1/2}\rho_\infty U_\infty{}^3} \text{ and } N_\Gamma = \frac{\bar{\alpha}_p \sigma \rho_\infty \bar{r}_b T_t{}^{4+b}}{\rho_\infty U_\infty{}^3} \tag{31}$$

into the right-hand sides of Eqs. (2, and/or 4 and 30), thus relating the energy forms to the common-freestream energy. The Mach number and altitude variance of the parameters N_α and N_Γ, representative of the flight corridor are provided in Table 1. Note that the level of convection and radiation is considerably less than the work related to pressure drag (which is directly proportional to the freestream energy $\rho_\infty U_\infty{}^3$) for much of the flight corridor, becoming significant in a relative sense at the higher Mach numbers and altitudes (in the Mach number range beyond that of Table 1, the radiative heating would become dominant.)

The necessary first-order differential equations for the Mayer problem formulation of the minimum energy-body shapes can now be summarized as:

$$\dot{\alpha} = N_\alpha (u/U_\infty) Z^2 r^{2j}/\eta^{1/2} \tag{32}$$

$$\dot{\eta} = (u/U_\infty) Z^2 r^{2j} \tag{33}$$

$$\dot{\beta} = Z^3 r^j \tag{34}$$

$$\dot{\Gamma} = r^j \lambda \tag{35}$$

$$\dot{\lambda} = N_\Gamma Z \bar{T}^{4+b}/\bar{u} \tag{36}$$

$$\dot{x} = (1 - Z^2)^{1/2} \tag{37}$$

$$\dot{r} = Z \tag{38}$$

where (u/U_∞) is provided by Eq. (21) and x and y have been added to account for the body shape itself. $\bar{T}$ and $\bar{u}$ are obtained after Eqs. (21, 23, 24, and 28) have been solved to provide the shock-layer properties. A numerical application of the maximum principle to the aforementioned equations will produce the desired optimum shapes.

Application of the Pontryagin Maximum Principle

The maximum principle serves to minimize some quantity $J = \varphi(x^f, t^f)$ subject to the differential constraints $\dot{x}_i = f_i(x, u)$, $i = 1, n$ the boundary conditions $x = x^0$ at $t = t^0$ and end constraints $\Psi_j(x^f, t^f) = 0$, $j = 1, mm < n$. The variables

Table 1 Variation of convective and radiative parameters with Mach number and altitude ($\gamma = 1.1$)

M_∞	Alt $\times 10^{-3}$	$N_\alpha \times 10$	$N_\Gamma \times 10$
5	50	0.013	10^{-9}
	100	0.040	10^{-9}
10	100	0.016	
	150	0.054	
15	120	0.023	0.571×10^{-3}
	180	0.096	0.692×10^{-2}
20	150	0.061	0.181
	200	0.132	0.316
25	200	0.139	7.85
	250	0.288	0.728
30	200		109.6
	250		10.0

x_i are referred to as state variables, u is the control variable (or variables), and t is the independent variable. In this context, the superscripts 0 and f refer to initial and final values, respectively, (i.e., initial and final in the range $t^0 \leq t \leq t^f$).

To apply the principle, it is necessary to introduce the adjoint variables obtained by

$$\dot{P}_i = -P_j \, \partial f_j/\partial x_i \quad i = 1,n \tag{39}$$

along with the transversality conditions

$$P_i + \mu_j \, \partial \Psi_j/\partial x_i + \partial \varphi/\partial x_i = 0 \qquad i = 1, n \; (t = t^f)$$
$$P_i f_i = \mu_j \, \partial \Psi_j/\partial t + \partial \varphi/\partial t \tag{40}$$

where μ_i are constants associated with the various end constraints ψ_j, and the Hamiltonian $H = P_i f_i = H(P, x, u)$ (repeated subscripts imply summation).

A minimum of J is obtained when the optimum control $u(t)$ is found which satisfies the condition

$$H(P, x, \tilde{u}) \geq H(P, x, u) \tag{41}$$

at every point on the trajectory. The numerical means of attaining this condition will be the method of steepest descent or the gradient method. Reference 15 provides the details of both the maximum principle and the gradient method.

Basically the procedure involves the assumption of an optimum condition or, equivalently, an assumed control function $u(t)$. Through the assumed control, the state variables $x_i(t)$ may be obtained by numerically integrating from the initial conditions x_0 through $(x(t^f))$ while satisfying the contraints $\Psi_j(x^f, t^f)$. The adjoint variables are then obtained by integrating Eq. (39) backwards, from t^f to t^0; the values of the adjoint variables at t^f are supplied by the transversality conditions [Eq. (40)]. The Hamiltonian can then be formed through changes in the control variable by

$$\delta u_i = (1/2\nu) P_j \, \partial f_j/\partial u_j \tag{42}$$

a new control can be determined such that $H(P, x, \tilde{u}) \geq H(P, x, u)$ where $u = \tilde{u} + \delta u$.

On obtaining the closer to the optimum control $u(t)$, a new family of state $x_i(t)$ and adjoint $P_i(t)$ variables is obtained. This procedure is repeated, adjusting the constants μ_i in Eq. (40) to satisfy the end constraints until the condition of Eq. (41) is satisfied throughout the range $t^0 \leq t \leq t^f$ or, equivalently, the gradient of Eq. (42) goes to zero, at which point the minimum values of J will be reached.

In the present problem, the independent variable is the arc length s and the state variables are $\alpha(s)$, $\eta(s)$, $\beta(s)$, $\Gamma(s)$, $\lambda(s)$, $x(s)$ and $r(s)$. The control variable is the local body slope $Z(s)$. The differential constraints are accordingly Eqs. (32–38). The nose shapes being considered must maintain a given fineness ratio. By stopping the numerical integration at a predetermined x value, it is necessary to impose only a single end constraint to maintain the desired fineness ratio, i.e.,

$$\Psi_1[r(s_f)] = r_f - 1 = 0 \tag{43}$$

Applying Eq. (39), the differential adjoint equations are

$$\dot{P}_1 = \dot{P}_3 = \dot{P}_4 = \dot{P}_6 = 0$$
$$\dot{P}_2 = P_1(u/U_\infty) Z^2 r^{2j}/2\eta^{3/2} \quad \text{and} \quad \dot{P}_5 = -P_4 r^j \tag{44}$$
$$\dot{P}_7 = -P_1 N_\alpha 2j(u/U_\infty) Z^2 r/\eta^{1/2} - P_2 2j(u/U_\infty) Z^2 r - jP_3 Z^3 - jP_4 \lambda$$

The quantities to be minimized, either alone or summed with another, are $\alpha(s_f)$, $\beta(s_f)$, and $\Gamma(s_f)$. Accordingly, $P_1(s_f)$, $P_3(s_f)$, and $P_4(s_f)$ are either -1.0 or 0.0, in accordance with Eq. (40) and the condition for which the body shape is being optimized. Table 2 lists the appropriate values for the various bodies being considered.

We obtain further from Eq. (40)

$$P_2(s_f) = P_5(s_f) = P_6 = 0 \tag{45}$$

Here $P_7(s_f) = -\mu_1$ where μ_1 is an undetermined constant that must be determined to satisfy the end constraint [Eq. (43)].

The initial assumed optimum shape is that of a blunted cone. The associated control variable $Z(s)$, the initial conditions $\alpha(s_0) = \beta(s_0) = \Gamma(s_0) = \lambda(s_0) = x(s_0) = r(s_0) = 0$, $\eta(s_0) = \eta_0 \neq 0$ (η_0 obtained by applying the L'Hospital rule to the integral of Eq. (32) under the condition $s \to 0$), and Eqs. (32–38) will then provide the family of state variables through the range $0 \leq s \leq s_f$. Choosing the appropriate values of $P_1(s_f)$, $P_3(s_f)$, and $P_4(s_f)$ from Table 2, together with conditions of Eq. (45), Eqs. (44) are integrated backwards, from $s = s_f$ to $s = 0$, to obtain the family of adjoint variables $P_i(s)$. Variations in the control variable are then obtained through Eq. (42) together with Eqs. (32–38) to provide

$$\delta Z = \frac{1}{2\nu}\left\{\left(\frac{P_1}{\eta^{1/2}} + P_2\right)\left[2\left(\frac{u}{U_\infty}\right)\frac{Zr^{2j}}{\eta^{1/2}} - 2\left(\frac{\gamma-1}{\gamma+1}\right)\left(\frac{u}{U_\infty}\right)^{-1} r^{2j} Z^{3\gamma-2/\gamma}\right] + P_3 3Z^2 r^j = P_5 \frac{\bar{T}^{4+b}}{\bar{u}} + P_7\right\} \tag{46}$$

(where ν is an arbitrary constant which helps to determine the control variation). Observing that the new control variable $\tilde{Z} = Z + \delta Z$ satisfies the condition of Eq. (41) at every point in the range $0 \leq s \leq s_f$, the control Z is replaced with $\tilde{Z}$ and a new family of state and control variables is generated. This procedure is repeated until further changes in the control fail to satisfy the maximum principle condition [Eq. (41)].

When the optimum-body shape being considered includes radiation effects, it is necessary to recalculate the shock-layer properties [through Eqs. (21, 23, 24, 28, and 30)] each time the body shape is changed through the adoption of a new control variable. This sequence was programmed for the IBM 7090 and the minimum drag, minimum heat, and minimum energy-nose shapes with a given fineness ratio were determined.

Table 2 Value of adjoint variables at $s = s_f$ for various optimum shapes

Variable	ϕ	$P_1(s_f)$	$P_3(s_f)$	$P_4(s_f)$
Minumum drag	$\beta(s_f)$	0.0	-1.0	0.0
Minimum heat (convective)	$\alpha(s_f)$	-1.0	0.0	0.0
Minimum heat (radiative)	$\Gamma(s_f)$	0.0	0.0	-1.0
Minimum energy (convective + drag)	$\alpha(s_f) + \beta(s_f)$	-1.0	-1.0	0.0
Minimum energy (convective + radiative)	$\alpha(s_f) + \Gamma(s_f)$	-1.0	0.0	-1.0
Minimum energy (convective + radiative + drag)	$\alpha(s_f) + \Gamma(s_f) + \beta(s_f)$	-1.0	-1.0	-1.0

Results and Discussion

Shock-Layer Solution

The numerical procedure used to provide the shock-layer temperature distribution was formulated to provide a solution that is both direct and rapid. These criteria are essential when it is realized that the shock-layer properties must be recalculated after each iteration which determines a new shape closer to the optimum. Despite its simplicity, the method shows reasonably good agreement with some of the more detailed numerical shock-layer solutions. Figure 3 compares present results with those obtained by Zlotnick and Neumann as indicated in Ref. 10. The greatest discrepancy between the methods is seen to be in the surface pressure distribution. The surface pressure obtained by the Zlotnick-Neumann method falls below that predicted by the Newtonian plus centrifugal (or Newton-Busemann) pressure relation which, in turn, is known to underestimate the pressure on a spherical body and leads to a fictitious free layer (negative-pressure coefficient) beyond approximately the 60° position on the sphere. The modified Newtonian pressure relation used in the present method is known to correlate very well with experiment on bodies of this sort. This being so, the surface-pressure distribution as shown by the Zlotnick-Neumann method should be somewhat higher and result in an even closer correlation between the surface velocity and shock-layer profiles. The radiation cooling effect on the shock-layer temperature distribution is shown in Fig. 4. The rapid temperature drop just inside the shock is seen to emulate the cooling effect shown by the more detailed numerical solution of Cheng and Vincenti.[16]

Optimum Shapes

The numerical results of the optimization procedure were in agreement with previous experience in dealing with the axisymmetric-minimum drag and minimum convective heat transfer bodies (Figs. 5). The given fineness-ratio minimum drag body is found to closely coincide with the ¾ power-law body predicted by direct application of the calculus of variations. The nose shape producing a minimum in convective heating is found to be flat faced, as in Refs. 5 and 6, but with a less sharp corner than that obtained by Aihara[6] using the calculus of variations. (Although the flowfield analysis of the present study was not detailed enough to account for such factors as separation and secondary shocks resulting from overexpansion, it does appear that the rounded corner is more desirable since it is less likely to produce such flow conditions and the associated local hot spots.)

The optimum-nose shape producing a minimum in radiative heating (Fig. 5, Curve C) is found to be conical in shape as predicted by a number of authors (e.g., Ref. 12). There is, however, a significant difference in that the conical tip is found to be cusp-shaped. Such a tip may be impractical from a materials standpoint, but it is a justifiable result from a gas dynamics point of view. The reasoning leading to the conical shape follows from the fact that a cone will avoid the high shock-layer temperatures and entropy layer associated with the normal or near-normal shock of the blunt body. The cusped tip carries this reasoning a step further since such a

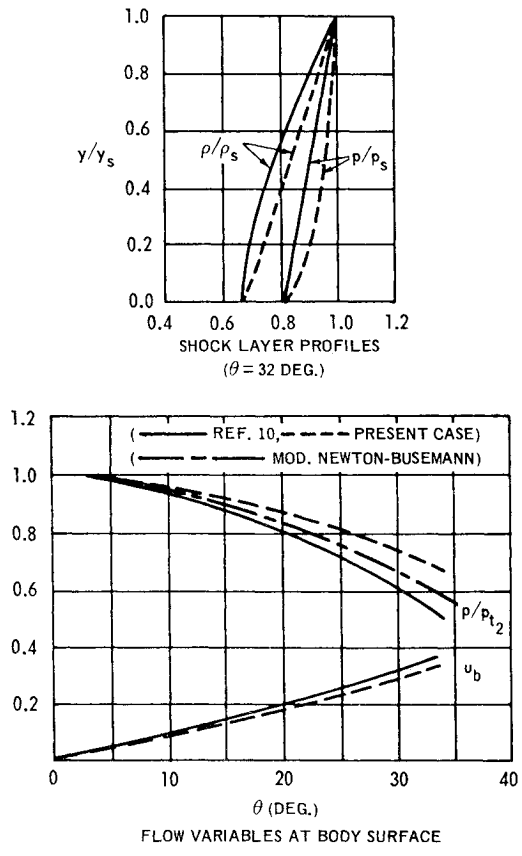

Fig. 3 Flow properties for spherical body $\gamma = 1.2$, $M_\infty = 10$.

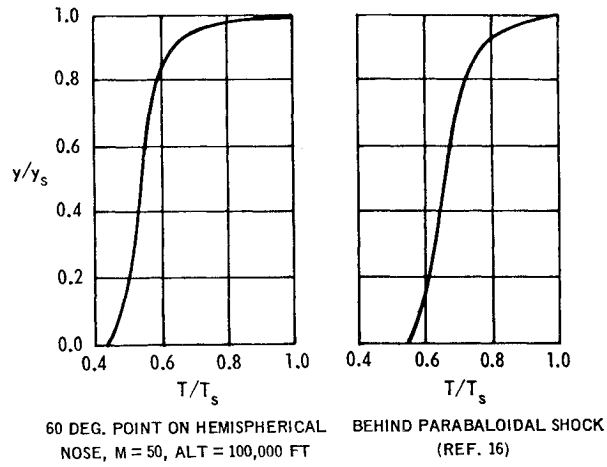

Fig. 4 Radiative-cooling effect on shock layer temperature distribution.

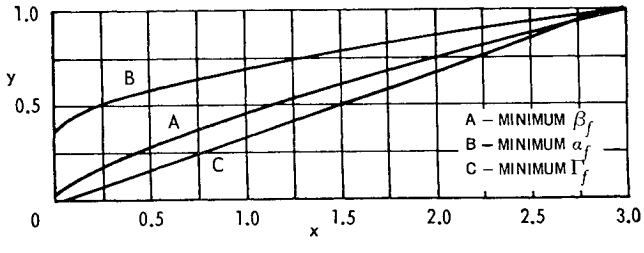

Fig. 5 Optimum nose shapes—axisymmetric (fineness ratio = 1.5).

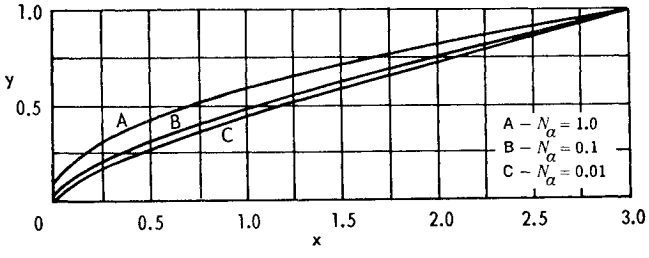

Fig. 6 Minumum energy-nose shapes considering convection and drag.

Table 3 Convective, radiative and drag variables related to axially symmetric nose shapes of fineness ratio 1.5

Case	Variable(s) being minimized	N_α	N_Γ	α_f	β_f	Γ_f
1	β_f	1.0	...	0.4310	0.0407	...
2	α_f	1.0	...	0.3880	0.0980	...
3	Γ_f	1.0	1.0	0.4720	0.0531	0.3×10^{-5}
4	$\alpha_f + \beta_f$	1.0	...	0.4200	0.0508	...
5	$\alpha_f + \beta_f$	0.1	...	0.1159	0.0420	...
6	$\alpha_f + \beta_f$	0.01	...	0.0836	0.0410	...
7	$\alpha_f + \beta_f + \Gamma_f$	1.0	1.0	0.4260	0.0505	0.0166
8	$\alpha_f + \beta_f + \Gamma_f$	0.1	0.01	0.1160	0.0410	0.3×10^{-3}
9	$\alpha_f + \Gamma_f$	1.0	1.0	0.4168	0.0651	0.0538

shape would result in a slightly more oblique shock than the pure cone, thereby giving lower shock-layer temperatures and less radiative heating to the body.

Table 3 shows the numerical values of the different variables for the various optimum shapes. (Because of the considerable increase in computing time when determining the radiation, effect, through Γ_f, this variable was not determined in those cases where it was not being considered in the optimization process). The value of the parameters N_α and N_Γ is of little consequence in the resulting configuration when a single variable is being minimized. Thus, the values of α_f and Γ_f are not representative of a particular flight condition but simply provide a reference in the first three cases of Table 3 to show the effect on one variable while minimizing another. It is apparent that the drag level is considerably more sensitive to shape changes than is convective heating.

As stated earlier, the minimum energy-nose shapes must be considered in a different light from the optimum shapes, wherein, a single quantity is being minimized. Specific freestream conditions must be considered here. However, before we proceed to specific conditions, it may be of interest to observe the effect of the various energy forms on the minimum energy shapes by assuming them to be of equal significance. This can be accomplished by letting $N_\alpha = N_\Gamma = 1.0$ in the optimization procedure. Fig. 6 (Curve A) shows the resulting minimum energy shape when considering the sum of convection heating and drag. The compromise is obvious in that the extent of the bluntness is reduced compared to the minimum convective heating profile, falling between it and the minimum drag shape. Table 3 shows the increase in both α_f and Γ_f over those of their respective optimum shapes. Curves B and C of Fig. 6, together with Table 3, shows the diminishing influence of convection on the minimum energy shape as N_α decreases to the levels associated with the actual flight corridor (see Table 1). It is apparent that the minimum energy shape is fast approaching that of the minimum drag profile.

The effect of radiation on the minimum energy shape is shown in Fig. 7. Curve A, obtained while giving the various energy terms equal weight by allowing $N_\alpha = N_\Gamma = 1.0$, shows the tendency toward the conical shape as discussed with regard to the minimum radiative heat-transfer body. When more realistic values of N_α and N_Γ are considered (Curve B), the profile approaches that of the minimum energy shapes, with an equivalent N_α, wherein radiation was not considered (Curve B of Fig. 6). The profiles are found to be identical except at the tip, where the flat portion of the minimum energy shape, without considering radiation, has been replaced with a conical tip. Table 3 shows a slight reduction in drag and a negligible penalty in convection, when the effects of radiation (Cases 5 and 8) are included.

The minimum energy concept considered to this point (i.e., what might be considered for the nose shape of a hypersonic-cruise vehicle) would appear to lose significance below a Mach number of about 20. Below this range, the drag levels determine the minimum energy shape. A more suitable approach in the lower Mach number range would be to specify the tolerable heat load and then by maintaining α_f at some given value determined from the specified heat load, to minimize the drag variable β_f. It seems certain that the resulting configuration would fall between the minimum energy nose shape of Fig. 6, Curve C and the optimum shape considering convection alone (Fig. 5, Curve B); radiation would, or course, not be considered in this Mach number range. That is, the extent of the flat-faced portion would depend on the expected heat load, with the contour following a power law variation from there to the base.

The minimum energy-nose shape considering convection and radiation simultaneously would be pertinent to a re-entry body wherein these heating forms would be of near-equal magnitude. Such conditions would exist in the vicinity of Mach 30, i.e., in the slightly superorbital-speed range. In this case, the parameters N_α and N_Γ would be nearly equal and may be taken as unity. The freestream conditions and Mach number are those at 250,000 ft and $M_\infty = 30$.

Figure 8 shows the resulting nose shape and Case 9 of Table 3 the related numerical results. The now familiar conical tip is again in evidence; the considerable heftiness of the nose shape is undoubtedly a result of attempting to maintain some bluntness as relief for the convective heating. A comparison of Fig. 8 and Curve A of Fig. 7 (where convection, radiation, and drag were considered) shows a similarity between the two and emphasizes the slenderizing effect of including the drag. In all cases, where it is considered, the

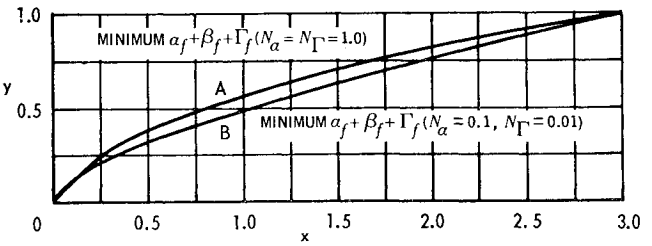

Fig. 7 Minumum energy-nose shapes considering convection, radiation, and drag.

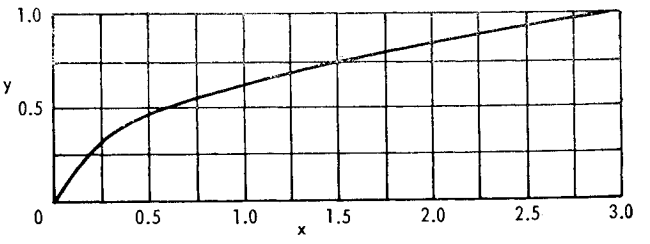

Fig. 8 Minimum energy-nose shape considering convection and radiation (minimum $\alpha_f + \Gamma_f$).

Table 4 Convective, radiative, and drag variables related to two-dimensional leading edge shapes of thickness ratio 1.5

Case	Variable(s) being minimized	N_α	N_Γ	α_f	β_f	Γ_f
11	β_f	1.0	...	0.8040	0.1002	...
12	α_f	1.0	...	0.7182	0.2160	...
13	$\alpha_f + \beta_f$	1.0	...	0.8066	0.1027	...
14	$\alpha_f + \beta_f + \Gamma_f$	1.0	1.0	0.7952	0.0993	0.4×10^{-4}

concession to the radiation effect is concentrated near the tip and is simply to create as slender a cone as the given case will allow, ranging from the rather blunt cone Case 9 (Fig. 8) to the cusp-tipped cone of Case 3 (Fig. 5, Curve C).

The two-dimensional optimum nose shapes are shown beginning with Fig. 9 with the related numerical values of the essential variables in Table 4. The minimum drag shape, Fig. 9 Curve A, is that of a wedge and, as in the axisymmetric case, is in agreement with what has been shown by direct application of the calculus of variations.[17] The minimum heat-transfer shape (convection) for the two-dimensional case, Fig. 9, Curve B, is found to be flat faced, as in the axisymmetric case, but with a less extensive expanse of flatness (Fig. 5, Curve B). This is significant when considered with the numerical values of Table 4. In going from the minimum drag shape of Case 11 to the minimum heat-transfer shape of Case 12, the reduction in α_f is seen to be on the order of 10% while the drag level has increased by better than 50%. It is evident then that the drag variation is even more sensitive to shape changes than was the case with the axisymmetric bodies. This being so, the minimum energy shapes are dominated by the drag terms and, as can be seen in Cases 13 and 14 of Table 4, the convective and radiative heating have little effect on the numerical values. For all practical purposes, the two-dimensional minimum energy shapes considering 1) convection and drag or 2) convection, radiation, and drag were wedge shaped as already shown in Curve A of Fig. 9. However, Fig. 10 is included to show the minimum energy shape for all three energy forms; with care, it is possible to detect a slight convex curvature in this figure.

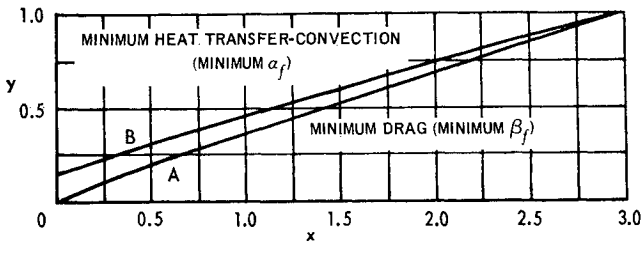

Fig. 9 Optimum nose shapes—two-dimensional (fineness ratio = 1.5).

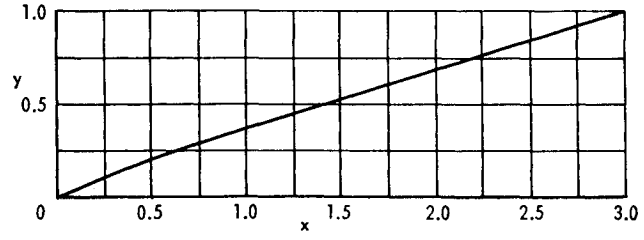

Fig. 10 Minimum energy leading edge shape considering convection, radiation, and drag (minimum $a_f + \beta_f + \Gamma_f$).

Conclusion

The optimum-hypersonic nose and leading edge shapes with a given fineness or thickness ratio were determined for a variety of optimizing criteria. The axisymmetric cases produced a near $\frac{3}{4}$ power law profile for the minimum drag shape and a flat-faced nose for the minimum heat transfer considering convection alone. When both convection and drag were considered, the minimum energy-nose shapes were flat faced, but with a less extensive expanse of flatness than the minimum heat-transfer noses. The influence of drag on the minimum energy shape was dominant at moderate hypersonic Mach numbers, suggesting an alternative approach at the lower Mach numbers, namely, specifying a given heat load and minimizing the drag. The results of this study indicate that such an approach would lead to similar flat-faced shapes with the expanse of flatness depending on the specified heat load.

When only radiation was considered, the optimum-nose shape was conical with a cusped tip, the cusped tip being an apparent attempt to produce a more oblique shock than the pure cone and therefore, lower shock-layer temperatures. When convection, radiation, and drag were considered, the minimum energy-nose shape was conical near the tip; the influence of radiation on the minimum energy shape was negligible except at the extreme Mach numbers that could be considered for a cruise vehicle (i.e., $20 \leq M \leq 25$). When only convection and radiation were considered, the minimum energy-nose shape had a large-angle conical tip. The conical tip provides relief from the severity of radiation and the blunting is retained to contend with convection.

The over-all results clearly illustrate the geometric means of alleviating the various energy forms. Drag reduction is produced by a slight degree of blunting near the tip, thereby reducing the body slope and therefore the pressure farther back on the body where the projected area (projected in the direction of the flight path) is greater. The effect of radiation is concentrated near the tip where the tendency is toward a cone so as to relieve the shock-layer temperatures. Convection tends toward the blunt body with its lower surface velocities and therefore lower shear.

The two-dimensional cases produced a wedge shape for the minimum drag profile and a flat face for the minimum heat transfer (convection). The extent of flatness on the minimum heat-transfer shape is considerably less than in the corresponding axisymmetric case. The drag is most susceptible to shape changes and is found to dominate when considered with the other energy forms. The result is that the two-dimensional minimum energy profiles are nearly wedge shaped in all cases considered.

References

[1] Miele, A., "The Calculus of Variations in Applied Aerodynamics and Flight Mechanics," D1-82-0113, June 1961, Boeing Scientific Research Lab., Seattle, Wash.

[2] Eggers, A. J., Jr., Resnikoff, M. M., and Dennis, H., "Bodies of Revolution Having Minimum Drag at High Supersonic Airspeeds," Rept. 1306, 1957, NACA.

[3] Allen, H. J., and Eggers, A. J., Jr., "A Study of the Motion and Aerodynamic Heating of Ballistic Missiles Entering the Earths' Atmosphere at High Supersonic Speeds," Rept. 1381, 1958, NACA.

[4] Hanawalt, A. J., Blessing A. H. and Schmidt, C. M., "Thermal Analysis of Stagnation Regions with Emphasis on Heat-Sustaining Nose Shapes at Hypersonic Speeds," *Journal of the Aerospace Sciences*, Vol. 26, May 1959, pp. 257–263.

[5] Furey, R. J., "Optimum Super/Hypersonic Leading-Edge Profiles," Rept. 2035, DDC AD 471 674, July 1965, Naval Ship Research and Development Center, Wash.

[6] Aihara, Y., "Optimum Body Geometries of Minimum Heat Transfer at Hypersonic Speeds," *AIAA Journal*, Vol. 6, No. 11, Nov 1968, pp. 2187–2189.

[7] Lees, L., "Laminar Heat Transfer over Blunt-Nosed Bodies at Hypersonic Flight Speeds," *Jet Propulsion*, Vol. 26, April 1956, pp. 259–269.

[8] Vincenti, W. G. and Kruger, C. H., Jr., *Introduction to Physical Gas Dynamics*, Wiley, New York, 1965, p. 538.

[9] Freeman, N. C., "On the Theory of Hypersonic Flow past Plane Axially Symmetric Bluff Bodies," *Journal of Fluid Mechanics* (*London*), Vol. 1, Oct. 1956, pp. 366–387.

[10] Hayes, W. D. and Probstein, R. F., "Inviscid Flows," *Hypersonic Flow Theory*, 2d ed., Vol. 1, Academic Press, New York, 1966.

[11] Wang, K. C., "Radiating Shock Layers," Research Rept. 67, June 1965, Martin Co., Baltimore, Md.

[12] Hoshizaki, H. and Wilson, K. H., "Viscous, Radiating Shock Layer about a Blunt Body," *AIAA Journal*, Vol. 3, No. 9, Sept. 1965, pp. 1614–1622.

[13] Maslen, S. H., "Inviscid Hypersonic Flow Past Smooth Symmetric Bodies," *AIAA Journal*, Vol. 2., No. 6 June 1964, pp. 1055–1061.

[14] "Equations, Tables, and Charts for Compressible Flow," Rept. 1135, 1935, NACA.

[15] McIntyre, J. E., "Guidance, Flight Mechanics and Trajectory Optimization," Rept. SID 65-1200-7 Vol. 7: *The Pontryagin Maximum Principle*, March 1968, North American Aviation, Inc, Downey, Calif.

[16] Cheng, P. and Vincenti, W. G., "Inviscid Radiating Flow over a Blunt Body," *Journal of Fluid Mechanics* (*London*), Vol. 27, March 1967, pp. 625–646.

[17] Chapman, D. R., "Airfoil Profiles for minimum Pressure Drag at Supersonic Velocities," Rept. 1063, 1952, NACA.